Interpretation of Airborne Spectral Reflectance Measurements Over Georgian Bay

J. R. MILLER, S. C. JAIN, N. T. O'NEILL,

Centre for Research in Experimental Space Science, York University, 4700 Keele Street, Toronto, Ontario M3J 1P3

W. R. MCNEIL,

W. R. McNeil and Associates, Inc., 47 Victoria Park Ave., Toronto, Ontario M4E 3S1

and K. P. B. THOMSON

Applications Section, Canada Centre for Remote Sensing, 717 Belfast Road, Ottawa, Ontario K1A OE4

Airborne spectral measurements were made along 3 flight lines over Georgian Bay in August and October 1974. Spectral data were collected in the wavelength regions 0.44 to 0.46 μm, 0.55 to 0.59 μm, 0.68 to 0.70 μm and 0.72 to 0.75 μm using a four-channel spectral scanning photometer. The airborne spectral reflectance curves over several stations were compared with subsurface volume reflectance measurements made as part of the Canada Centre for Inland Waters 1974 Lake Huron-Georgian Bay ship cruise. These comparisons permitted an evaluation of the water surface reflection effects on the airborne data. The airborne spectral reflectance curves are then interpreted using a two-flow radiative transfer model to derive chlorophyll concentration line profiles. Correlation coefficients between calculated and ship-measured chlorophyll data range from 0.810 to 0.984.

1. Introduction

The evidence of the correlation of water color changes with variations in the water chlorophyll concentration were reported in color index measurements (e.g. Jerlov (1968)) and in spectral reflectance measurements (Clarke et al. (1970)). These reports were followed by efforts to empirically arrive at a unique relationship between spectral reflectance ratios (color indices) and chlorophyll concentration (e.g. Arvensen et al. (1971), McNeil et al. (1976), Miller et al. (1973, 1976) and Ramsey and White (1973)). Empirical approaches to this problem have shown only limited success due to variations in observing conditions and perhaps more important because of the effect of the interrelationship of the scattering and absorption properties of the water medium on the observed spectral reflectance (or water color).

Various radiative transfer models have also recently been applied to the ocean, e.g. Gordon (1973), Gordon and Brown (1973), Kattawar and Humphreys (1976) and McCluney (1974) to compute the spectral reflectance expected from various backscattering probability functions and absorption coefficients. More recently, Jain and Miller (1976) have com-

bined an ocean-color model with an optimization method so that observed spectral reflectance curves can be interpreted in terms of chlorophyll concentration and the Mie scattering coefficient. The model provides a physical understanding for the observed reflectance curves.

This paper reports on spectral measurements made in collaboration with the 1974 CCIW Lake Huron-Georgian Bay Survey cruise. The airborne spectral reflectance data is interpreted using a two-flow ocean color model and is compared to ship data.

2. The Physical Basis for Interpretation of the Airborne Spectral Data

For an airborne passive optical sensor the radiance signal received at altitude z is normally written in the form

$$L_z(\lambda) = L_0(\lambda)T_a(\lambda) + L_a(\lambda), \qquad (1)$$

where $L_z(\lambda)$ is the apparent radiance of the earth's surface at wavelength λ and at altitude z, $L_0(\lambda)$ is the radiance at the earth's surface, $T_a(\lambda)$ is the atmospheric transmittance at λ and $L_a(\lambda)$ is the radiance signal generated by insolation back-scattered by the atmosphere. Because of the effects of atmospheric absorption and scattering, $L_z(\lambda)$ can differ significantly from $L_0(\lambda)$, especially for observations made at high altitudes. Moreover, in the case of measuring the radiance over a water surface, $L_0(\lambda)$ must be considered as the sum of (1) the inherent radiance $L_u(\lambda)$ (the radiance transmitted upward from beneath the water surface) and (2) $L_{rd}(\lambda)$ the radiance generated by Fresnel reflection of sky light and possibly a surface-reflected direct solar input component $L_{rs}(\lambda)$. The inherent radiance is the quantity whose spectral variation yields information about the water medium. (The radiance contribution from reflection from the lake or ocean bottom may also be important in certain cases).

In order to derive the inherent spectral reflectance of a scene using a passive optical sensor, it is desirable to make continuous measurements of the solar irradiance so that one can account for the spectral and intensity variability of the natural source incident solar radiation. Alternatively, under clear sky observation conditions it may be justified to neglect in-flight solar insolation variations and simply make pre-flight and postflight solar measurements. In this case, if our optical sensor were to observe a perfect Lambertian diffuser (100% reflectance) on the ground, the measured radiance $L_{s0}(\lambda)$ would be related to the total incident irradiance $H_0(\lambda)$ by:

$$L_{s0}(\lambda) = \frac{H_0(\lambda)}{\pi}, \qquad (2)$$

where the total incident solar irradiance $H_0(\lambda)$ is made up of a collimated direct-sun component $H_{0s}(\lambda)$ and a diffuse skylight component $H_{0d}(\lambda)$. The ratio of the upwelling radiance from the scene to the radiance from the perfect diffuser

$$R_{az} = \frac{L_z(\lambda)}{L_{s0}(\lambda)}, \qquad (3)$$

is called the apparent reflectance since it represents the reflectance of the scene as observed by the sensor at altitude z without corrections for atmosphere or surface effects.

The apparent spectral reflectance $R_{az}(\lambda)$ may be written in a more detailed form through equations (1), (2) and (3) by expressing the surface radiance L_0 as $L_u + L_{rd} + L_{rs}$ and letting F represent the diffuse sky component H_{0d} as a fraction of the total solar irradiance so that H_{0d} equals FH_0 and H_{0s} equals $(1\text{-}F)H_0$:

$$R_{az}(\lambda) = T_a(\lambda)\left[\frac{L_u(\lambda)}{L_{s0}(\lambda)} + \frac{L_{rd}(\lambda)\pi F}{H_{0d}(\lambda)} + \frac{L_{rs}(\lambda)\pi(1\text{-}F)}{H_{0s}(\lambda)}\right] + \frac{L_a(\lambda)}{L_{s0}(\lambda)}. \quad (4)$$

The surface reflectance can be defined according to Eq. (3) so that the surface reflectance for diffuse radiation r_{0d} is given by $L_{rd}\pi/H_{0d}$ and direct radiation r_{0s} is $L_{rs}\pi/H_{0s}$. The Fresnel water reflection coefficient for normal incidence r_0 is of special interest because for a nadir-viewing optical sensor r_{0d} is simply given by r_0. However r_{0s} for the nadir-viewing sensor is a strong function of the solar zenith angle and the wave state of the surface so that it is useful to represent r_{0s} by $r_0 f$ where f is a factor which accounts for the departure from a zenith sun and a perfectly smooth sea surface. Accordingly the apparent spectral reflectance for nadir-viewing is

$$R_{az}(\lambda) = T_a(\lambda)\left[\frac{L_u(\lambda)}{L_{s0}(\lambda)} + r_0 F + r_0(1\text{-}F)f\right] + \frac{L_a(\lambda)}{L_{s0}(\lambda)} \quad (5)$$

It is the inherent reflectance of the scene $L_u(\lambda)/L_{s0}(\lambda)$ which can be directly related to the volume reflectance R_v referred to in McNeil and Thomson (1974) that is fundamentally related to the absorption and scattering properties of the water medium. Ideally, one should determine all the other parameters in Eq. (5) to derive the inherent reflectance.

By making the airborne measurements at low altitudes (at 1500 feet in this project) it may be reasonable to assume $T_a(\lambda) = 1.0$ and also possibly $L_a(\lambda) = 0$. Then the apparent reflectance is represented simply by:

$$R_{az}(\lambda) \simeq \frac{L_u(\lambda)}{L_{s0}(\lambda)} + r_0 F + r_0(1\text{-}F)f, \quad (6)$$

which consists of the inherent reflectance plus two reflectance terms which arise from specular reflection of sky light and from specular reflection of direct sunlight. Under clear sky conditions the importance of the skylight reflectance may be estimated using data by Jerlov (1968) to obtain F as a function of the solar elevation angle and using the Fresnel reflection coefficient $r_0 = 0.02$ for nadir-viewing. Under completely overcast conditions ($F = 1$) this term equals

2%, a very significant addition to the inherent reflectance term. The direct-sun specular reflection is normally minimized by planning field observations when the solar zenith angle is sufficiently large (30° for this project) to avoid viewing the surface glitter zone. The effectiveness of this technique is a function of the solar zenith angle and the sea state, the variability of which is accounted for by f in Eq. (6). In practice, it is desirable to determine this term directly through field measurements.

3. Instrumentation

The principal airborne sensor used for this study was a four-channel spectral-scanning photometer. The photometer measures simultaneously the upwelling spectral radiance in four spectral bands; in addition, it is capable of spectral scanning four different spectral regions, each up to 400Å in extent, at a resolution of about 30Å. Figure 1 shows the 15 spectral response curves for each of the four photometer optical channels. One complete spectral scan requires about 4 seconds during which the scene is viewed in 60 spectral bands. (A more complete description of the spectral-scanning photometer design can be found in Miller et al. (1972) and Gordon (1975)). For the present experiment, interference filters were chosen to study four important spectral regions: (1) ~0.46 μm where the chlorophyll a absorption is near maximum (2) ~0.56 μm where chlorophyll a absorption is low and water penetration is high, (3) ~0.70 μm and (4) ~0.75 μm to respond to changes in water turbidity and/or plant material floating on the water. As shown in Fig. 1, this photometer design provides spectral information in the spectral regions 0.44 to 0.46 μm, 0.55 to 0.59 μm, 0.68 to 0.70 μm, and 0.72 to 0.75 μm at a resolution of about 30Å (0.003 μm).

A disadvantage of this photometer design is that the motion of the aircraft causes a continual change in the scene as observed by the nadir-viewing photometer during the 4 second spectral span. With the airborne measurements carried out at 1500 feet (457 m), the photometer 15° full angle field of view results in a scene diameter on the water surface of 390 feet (118 m). At typical airspeeds of 200 ft/sec the photometer field-of-view traverses 2 scene diameters during each spectral scan. So to obtain valid spectral data in all 60 photometer spectral elements it is necessary to assume that the average water optical properties within a 390 foot scene diameter change very little between adjacent scene diameters. Previous data and present data (see Sec. 5.1) show this to be a valid assumption for most lake water measurements; however, in coastal regions where large variations are often observed within 100 feet this instrumental feature would significantly limit the usefulness of the data. It is important to note that at each step of the photometer, upwelling spectral radiance measurements are made simultaneously in four passbands for 100 msec during which time the airplane moves only 20 feet. Therefore, if the data is required from *only 4* passbands, valid spectral radiance data can be obtained at 4 second intervals without assumptions about spatial homogeneity.

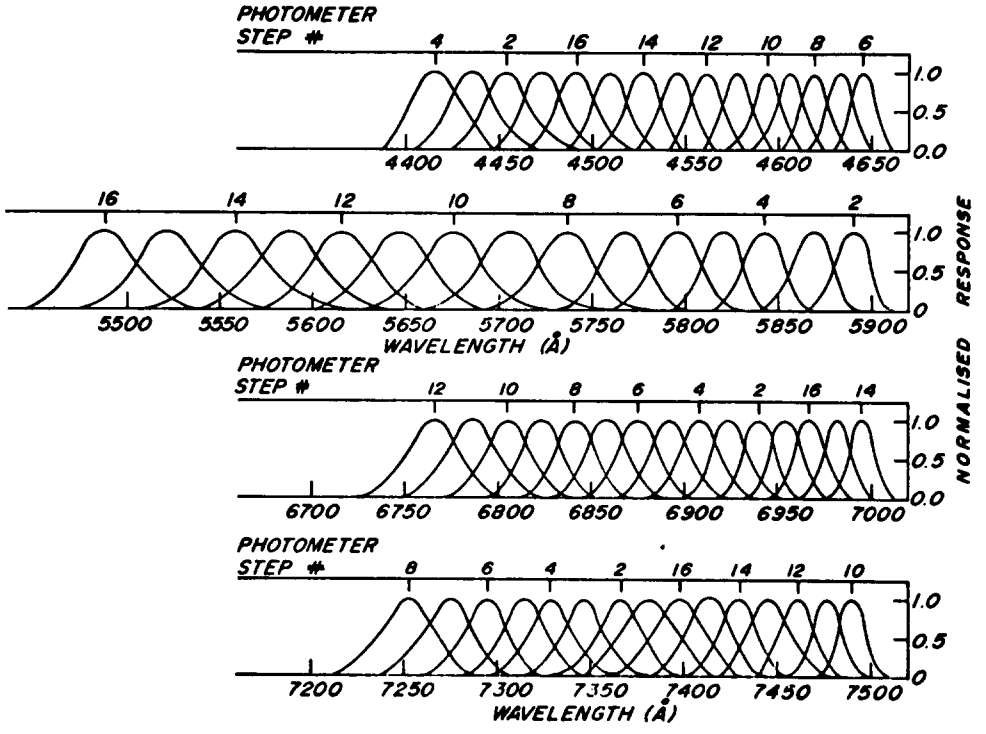

FIG. 1. The photometer instrumental response curves.

4. Field Measurements

Flights were planned over selected portions of the Canada Centre for Inland Waters (CCIW) 1975 Lake Huron and Georgian Bay Survey cruises. The network of ship sampling stations on Georgian Bay and the three flight lines flown are illustrated in Fig. 2.

The photometer was flown on board a Canada Centre for Remote Sensing (CCRS) DC-3 aircraft specially instrumented for remote sensing work. Each flight was subject to the flight criteria of 1500 feet flight altitude, less than 10% cloud cover and solar elevation between 30° and 60°. Flights made on August 7 and October 11, 1974 will be reported on in this paper.

Because this photometer is not capable of in-flight solar irradiance measurements, pre-flight and post-flight solar calibrations were made at Malton Airport and Wiarton Airport. The photometer was then taken out on the runway about 30 feet from the aircraft and directed obliquely at a horizontally oriented Lambertian white diffuser (an aluminum plate coated with Eastman Kodak Standard 100% White Reflectance Paint (Grum & Luckey (1968)). Then, through Eq. (3) these measurements provide the basis for calculating the apparent spectral reflectance from the airborne spectral radiance data.

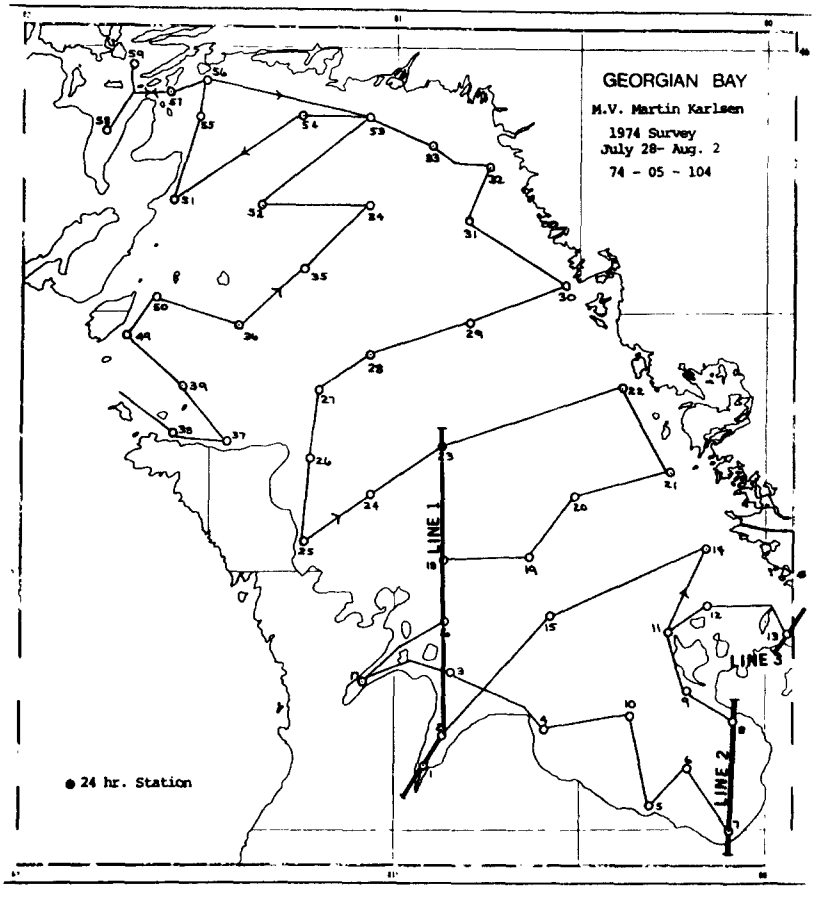

FIG. 2. Georgian Bay CCIW ship sampling stations and the three selected flight lines.

A scanning spectrometer (AB Incentives Quanta meter) was used to measure the upwelling and downwelling irradiance in the 400 nm to 700 nm spectral region at a depth of about 1 meter. These subsurface irradiance spectral reflectance measurements (that is, the ratio of upwelling to downwelling irradiance $R_v(\lambda)$) were made at selected cruise stations (whenever possible) as part of the ship-based water quality measurement program. The subsurface irradiance reflectance data $R_v(\lambda)$ can be related to the above-surface irradiance reflectance $R'_v(\lambda)$ by the approximate simple relationship $R'_v(\lambda) \simeq 0.52\, R_v(\lambda)$ (Austin (1974), McNeil & Thomson (1974)); this relationship accounts for the effect of the internal reflection at the water-air interface arising from the change in index of refraction. If we consider the water back-scattered radiation to be isotropic then the calculated above-surface irradiance reflectance $R'_v(\lambda)$ should be equal to the inherent water radiance reflectance $L_u(\lambda)/L_{s0}(\lambda)$ determined from the air-

based data. Therefore, at a particular station, comparison of the airborne spectral reflectance curve with that derived from the in situ irradiance reflectance should differ only because of surface specular reflection and atmospheric path radiance effects. Consequently, such comparisons permit these effects to be evaluated for each of the cruise over-flights.

The ship-based chlorophyll concentration data were obtained from 0 to 20m integrated samples at each of the monitoring stations.

5. Presentation and Interpretation of Airborne Data

The photometer output signals, which were recorded on board with an analog instrumentation tape recorder, were digitized and used to derive data files of apparent reflectance. The desired parameter, the inherent water reflectance, differs from the derived apparent reflectance due to the specular reflection terms (see Eq. (6)).

Under clear sky conditions the specular reflectance due to skylight may be readily calculated. In the absence of diffuse/global solar radiation field measurements, data from Jerlov (1968) were used to provide the diffuse/global solar irradiance ratio F as a function of wavelength and solar zenith angle which was combined with a Fresnel reflection coefficient r_0 of 0.02 for nadir-viewing to evaluate the correction term r_0F ranging from 0.0016 to 0.0056 for the data presented. This small correction was applied to all the data during the processing resulting in data files of the reflectance

$$R'_{az} = \frac{L_u(\lambda)}{L_{s0}(\lambda)} + r_0(1\text{-}F)f. \qquad (7)$$

5.1 Apparent Spectral Reflectance Curves

An overview of the data available on a particular flight line is provided by plotting the apparent spectral reflectance curves as shown in Fig. 3. A series of similar spectral reflectance curves are shown with a regular displacement between curves. The solid part of each curve represents the spectral reflectance data from the photometer and the dashed lines are added to aid the eye in following a particular spectral curve. Starting at the top of the figure, the first curve represents the reflectance spectrum obtained with the sensor viewing the shore near Owen Sound; the left upper most cross is the corresponding axes intersection for this plot with the vertical scale being % albedo (or reflectance) as indicated on the left side of the plot and the wavelength in nanometers as the horizontal axis. In order to present all the Line 1 data on one graph each reflectance curve represents the average of 7 photometer spectral scans. In order to make successive spectral reflectance curves distinguishable, each successive curve is plotted with its vertical axis shifted downward to the next cross. Therefore, with Line 1 flown in a northward direction, successive curves going down in Fig. 3 represent reflectance spectra starting in Owen Sound and ending in the middle of Georgian Bay at Station 23.

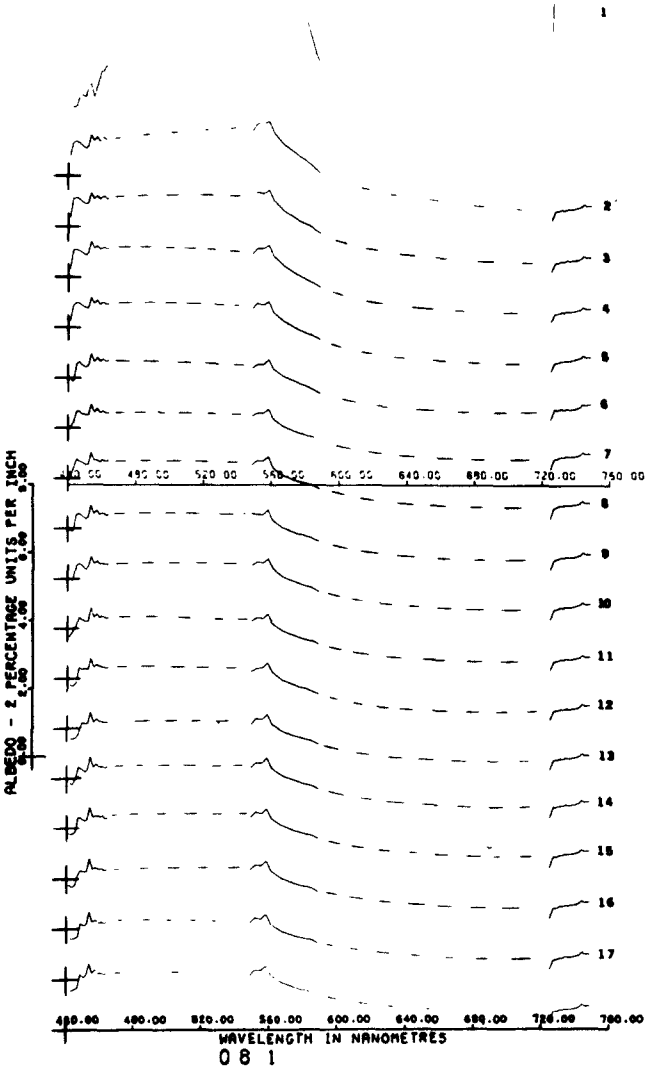

FIG. 3. Reflectance spectra along line #1 for the August Flight/CCIW Cruise #74-05-104.

A significant difference is apparent between reflectance curves 1 and 2. The most dramatic difference occurs in the near infrared region (0.72 to 0.75 μm) where the reflectance for curve 1 is about 15% (off-scale in Fig. 3) compared to about 1.7% in curve 2; this difference is characteristic of the high reflectance of vegetation on shore compared to the low reflectance of water in the near infrared. In fact, this dramatic near infrared reflectance change provides a convenient event marker in the data to signal the transition from shore to water. The

spectral curves from 3 to 18 over the water show almost imperceptable change; that is, there appear to be no large, significant anomalies in water optical properties along Line 1. Although the successive reflectance curves in Fig. 10 represent 7 photometer scan averages, a detailed scan-by-scan examination yields the same conclusion—no significant changes with the photometer 390 foot field of view.

5.2 August Flight—CCIW Cruise #74-05-104

The presentation of the August data is prefaced by the comment that the overflight for this cruise was not possible until six days after the ship cruise was completed. However, generally clear weather conditions prevailed over this period.

The photometer apparent reflectance spectrum $R'_{az}(\lambda)$ obtained over the mid-lake Station 23 is shown in Fig. 4(a) along with (1) the ship-based in situ measurement of the subsurface irradiance spectral reflectance, $R_v(\lambda)$, shown as the upper solid curve and (2) the above-surface inherent spectral reflectance $R'_v(\lambda)$, shown as the lower solid curve, which is inferred from the in situ volume reflectance data (i.e. $R'_v \simeq 0.52R_v$). In the near infrared region the ship-based optical data indicates that the above-surface reflectance originating from upwelling subsurface radiance is expected to be 0.1% compared to the apparent reflectance of 0.6% measured by the photometer. At these wavelengths it appears that about 80% of the signal observed by the photometer arises from solar specular reflection and/or atmospheric backscatter. The 0.5% difference in reflectance has been interpreted as solar glitter (represented by the term $r_0(1\text{-}F)f$ in Eq. (2.6) and/or atmospheric backscatter. Accordingly, it is assumed that the subtraction of 0.5% from the apparent reflectance results in the desired inherent spectral reflectance $L_u(\lambda)/L_{s0}(\lambda)$.

According to the above interpretation one would expect that the apparent reflectance spectrum should be simply displaced from $R'_v(\lambda)$ by 0.5%; however, it is noted that this is true instead for $R_v(\lambda)$ and that the shape of $R'_v(\lambda)$ and $R'_{az}(\lambda)$ do not in fact agree very well. The reason for this discrepancy is not clear. Although this disagreement between the ship and airborne spectral reflectance data remains unresolved, the surface reflection correction term determined by examining the near infrared reflectances can reasonably be accepted as a valid measurement since $R'_{az}(0.7)/R'_v(0.7) \sim 6$.

The photometer reflectance data obtained on Line 1 on August 7, 1974 is shown in Fig. 5(a). The spectral reflectance curves given in Sect. 5.1 were shown to be slowly-varying smooth functions. Therefore, to simplify the data manipulations, reflectance data at only four wavelengths R'_{az}(4524 Å), R'_{az}(5560 Å), R'_{az}(6995 Å) and R'_{az}(7430 Å), one in each of the spectral regions scanned, were selected for detailed study. The photometer obtains reflectance data at these four wavelengths simultaneously when the photometer mask is in position 14 (see Fig. 1). Thus, the photometer yields a reflec-

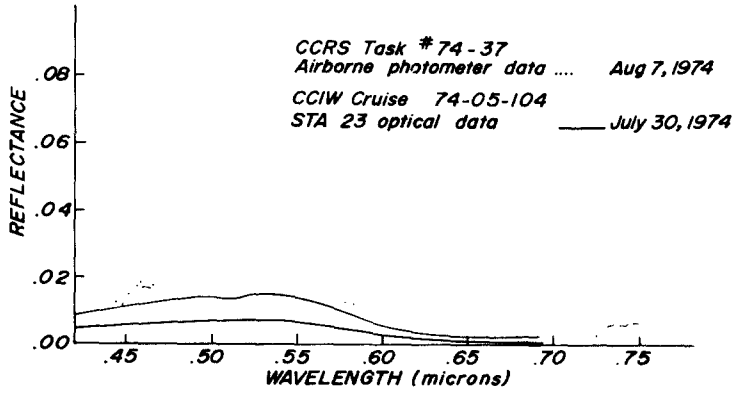

FIG. 4(a). Comparison of remotely-measured radiance spectral reflectance to the ship-based irradiance spectral reflectance data at station 23. The upper solid curve represents the in situ volume reflectance data whereas the lower solid curve indicates the expected spectral reflectance for above the water surface.

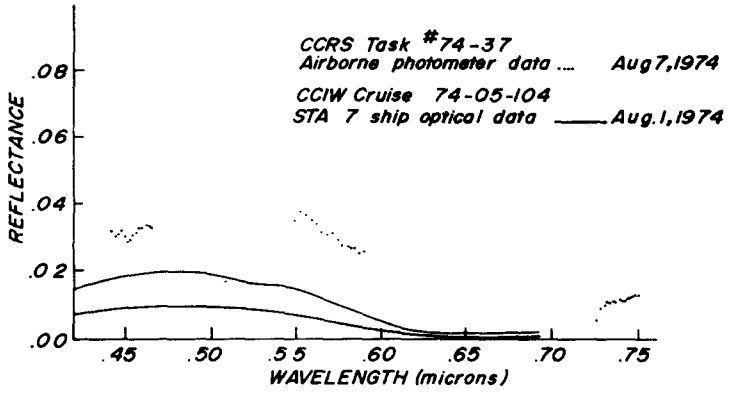

FIG. 4(b). Comparison of remotely-measured radiance spectral reflectance to ship-based irradiance spectral reflectance data at station 7.

tance measurement at these four wavelengths once per scan (every 4 seconds). These reflectances are plotted as a function of the accumulative scan (or frame) number, which is related to distance along the track and the corresponding water depth in the middle figure.

The reflectance line profiles at three wavelengths (one photometer channel malfunctioned) in Fig. 5(a) indicate significant reflectance changes only in the near-shore area in Owen Sound. Along the remainder of the flight line the reflectance decreased slowly (except for

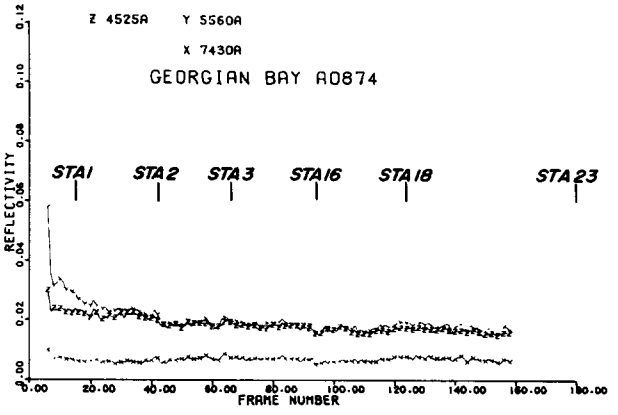

FIG. 5(a). Reflectance line profiles for Line #1 on the August Flight/CCIW Cruise #74-05-104.

the 7430Å channel) toward the mid Georgian Bay region. It is noted that large spatial variations in the water reflectance were *not* observed.

Now using the surface reflection correction term derived from Fig. 4a the resulting inherent spectral reflectance was applied to two-flow model of Jain and Miller (1976) to compute a line profile of chlorophyll concentration and the Mie Scattering coefficient shown in Fig. 5(b). The corresponding ship-based chlorophyll data at each of the monitoring stations is indicated by the dots.

The point-to-point fluctuations in the computed chlorophyll line profile arises partially from the small variations in the reflectance data and partially from the finite time alloted to the optimization routine.

The Line 2 data were also analyzed in a manner similar to that described above and are presented in Fig. 6. The reflectance line profiles show significant reflectance changes at 4525 Å and 5560 Å in the near shore regions which are probably due mainly to bottom reflectance effects since the 7430 Å reflectance shows no corresponding change over these water regions. The surface reflection correction term derived from Fig. 4(b) (as for Station 23) has been used in the water-color interpretation program to compute the expected chlorophyll concentration line profile shown in Fig. 6(b). The comparison with the ship chlorophyll data and an examination of the large differences between the ship and airborne spectral reflectance curves indicate that significant water quality changes occurred at these relatively shallow stations during the period between the ship and airborne measurements.

The analysis of Line 3 data is summarized in Fig. 7. The anomaly in the reflectance profile at scan number 5 is the result of crossing part of Beausoleil Island. The comparison of computed and measured chlorophyll concentration at Station 13 is shown in Fig. 7(b).

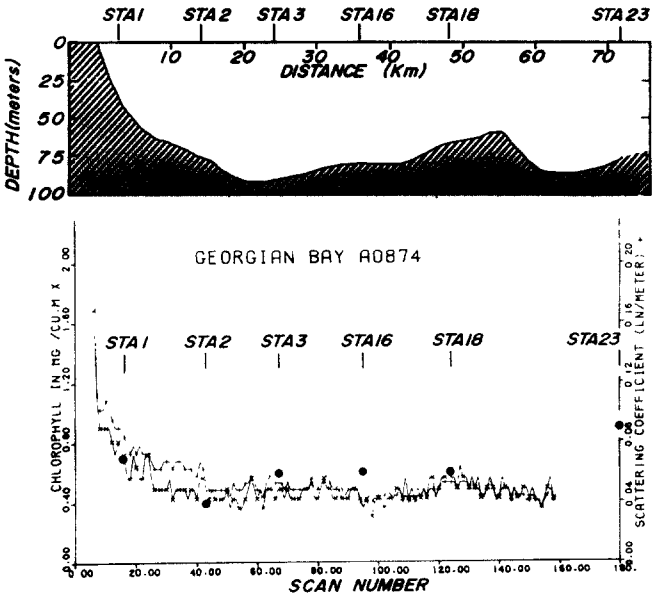

FIG. 5(b). Computed chlorophyll concentration line profile for line 1 compared to the measured station chlorophyll values (shown as dots) obtained on the CCIW Cruise #74-05-104.

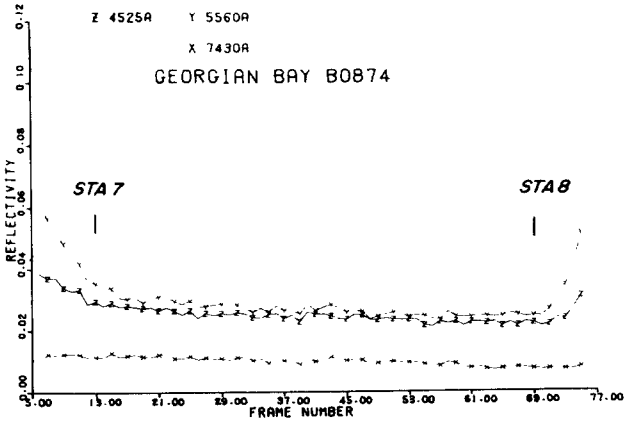

FIG. 6(a). Reflectance line profiles for Line #2 on the August Flight/CCIW Cruise #74-05-104.

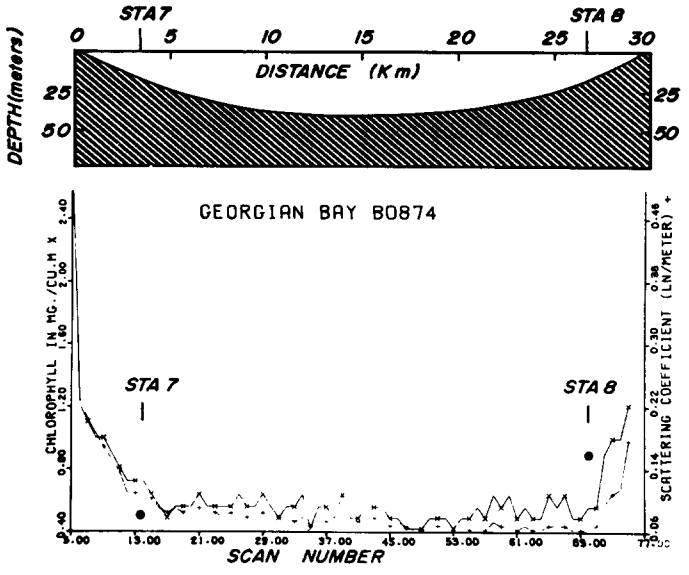

FIG. 6(b). Computed chlorophyll concentration line profile for line #2 compared to the measured chlorophyll values (shown as dots) obtained on CCIW Cruise #74-05-104.

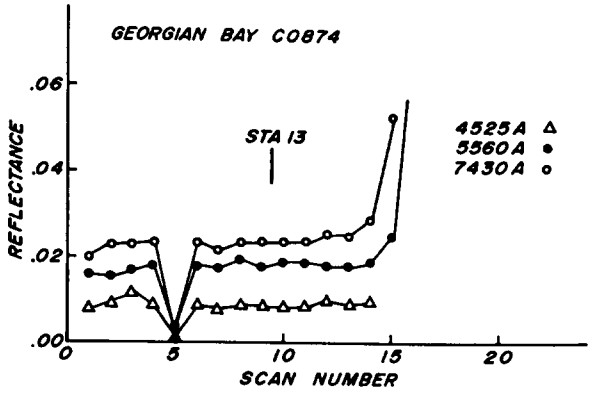

FIG. 7(a). Reflectance line profiles for Line #3 on the August Flight/CCIW Cruise #75-05-104.

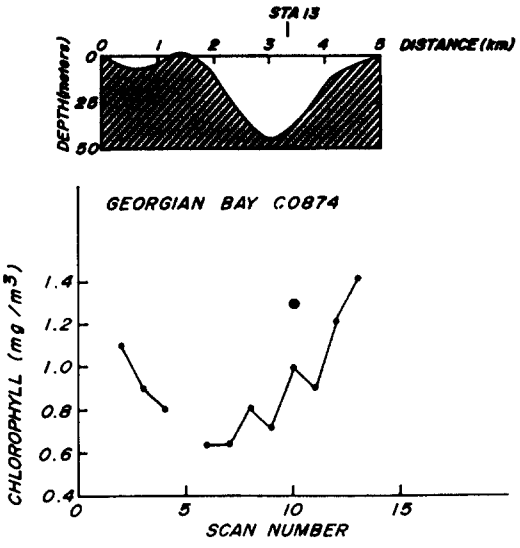

FIG. 7(b). Computed chlorophyll concentration line profile for Line #3 compared to the measured chlorophyll value at station #13 obtained on the CCIW Cruise #74-05-104.

5.3 October Flight–CCIW Cruise #74-05-106

The October overflight provides airborne data which is time-delayed from the ship data between 1 and 3 days. The reflectance profiles for Line 1 are presented in Fig. 9. These curves show considerably more variation along the flight line than that observed in the August data.

Of all the water monitoring stations that were overflown, ship-based optical measurements were made on only Stations 2 and 23, both on Line 1. The ship-based and airborne spectral reflectance data for Stations 2 and 23 are shown in Fig. 8(a) and 8(b), respectively. Both spectrum comparisons indicate a solar specular reflection component of about 1.3%; this significant solar glitter problem was evident in the aerial track-recovery photography. The 1.3% surface reflection correction term obtained from Fig. 8 was used in the water-color interpretation program to calculate the expected Line 1 chlorophyll concentration line profile shown in Fig. 9. Agreement is found within about 30% between the remote sensing determinations and the ship-based chlorophyll measurement.

6. Discussion and Conclusions

A summary of the comparison of the ship-based chlorophyll concentration measurements with those derived from the analysis of airborne spectral reflectance data from this Georgian Bay project is shown in Fig. 10. The correlation coefficient for all the data is 0.810. Circled data points indicate probable interpretation errors because of bottom reflection signal contributions for the shallower Stations 7, 8 and 13. If these data are excluded the correlation coefficient becomes 0.948. Spectral data has been previously investigated by Jain et al. (1975) for a larger range of measured chlorophyll values, from 0.6 to 18 mg/m^3. For these data a correlation coefficient of 0.986 was found. These correlations suggest that physical modelling has reached a stage where quantitative water parameters can be derived by remote sensing means with useful accuracy.

Although this scanning photometer provided reflectance in 60 spectral channels the present data suggest that airborne radiometric measurements in

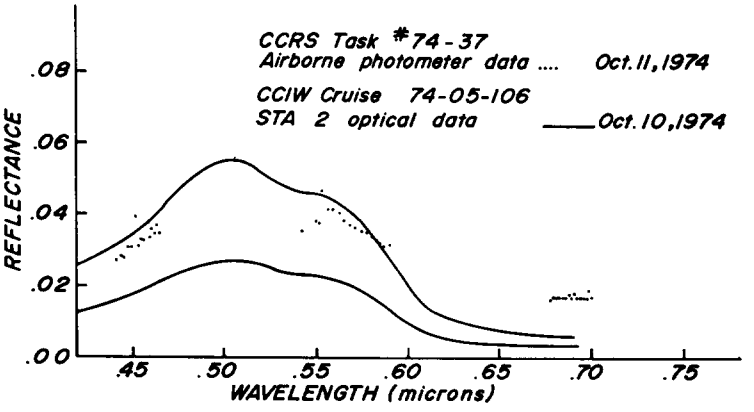

FIG. 8(a). Comparison of remotely measured radiance spectral reflectance to the ship-based irradiance reflectance at station 2.

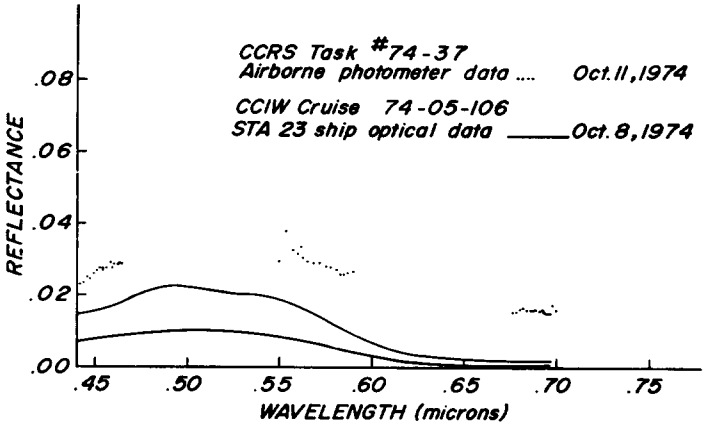

FIG. 8(b). Comparison of remotely measured radiance spectral reflectance to the ship-based irradiance spectral reflectance at station 23.

only 4 spectral channels, selected in the appropriate wavelength regions, can provide useful water quality information. The importance of this result lies in the feasibility of using simpler instrumentation with less demanding data analysis requirements for routine optical water quality monitoring.

The analysis of this data has illustrated the importance of making a field measurement of the surface reflection component of the radiance signal as observed at aircraft altitudes. The comparison of airborne and in situ reflectance data in the near infrared ($\sim 0.7\mu m$) showed that most of the observed signal originated from the surface. These measurements demonstrate the validity of the use of optical measurements in the near infrared to determine the specular reflectance

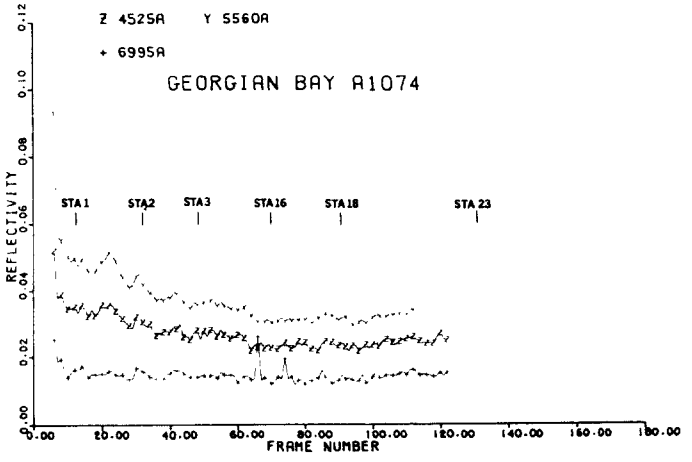

FIG. 9(a). Reflectance line profiles for Line #1 on the October Flight/CCIW Cruise #74-05-106.

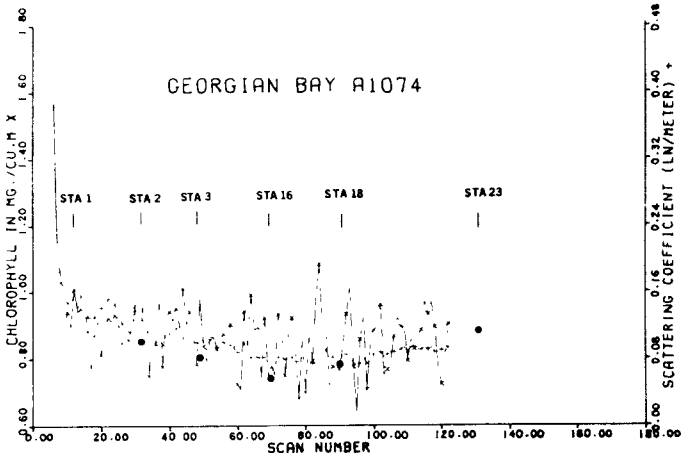

FIG. 9(b). Computed chlorophyll concentration line profile for Line #1 compared to the measured chlorophyll values (shown as dots) obtained on the CCIW Cruise #74-05-106.

signal. For turbid water one would expect the upwelling signal to form a much more important part of the apparent reflectance at 0.7 μm so that a measurement near 0.97 μm, at the water absorption maximum, should provide a more effective use of this technique to determine the specular reflectance.

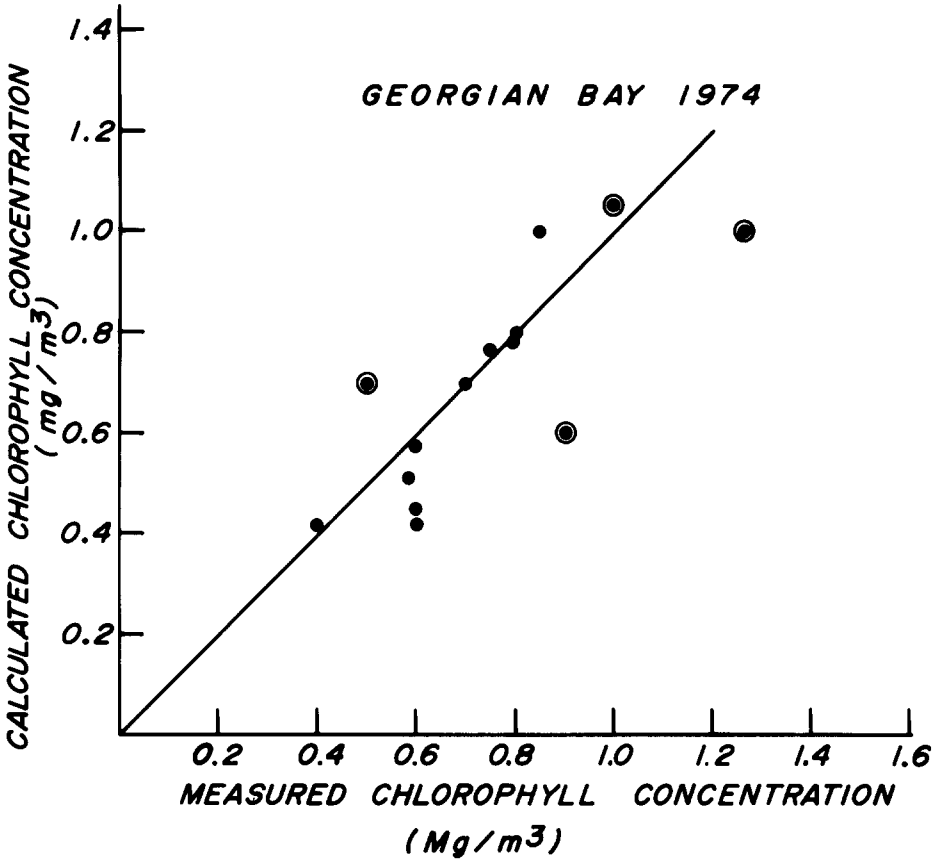

FIG. 10. Correlation curve for the computed and measured chlorophyll concentrations obtained from the Georgian Bay overflights. The data points in which contamination by bottom reflectance was evident are indicated by circled dots.

This work was possible because of the support of the Canada Centre for Inland Waters through DSS contract #0554-0078. The authors are grateful to Dr. K. S. Gordon who contributed a great deal to the analysis of this data and to the personnel of the Data Acquisition Section of CCRS, the Airborne Sensing Unit of the Canadian Armed Forces and to the personnel involved in the data collection on the ship M. V. Martin Karlsen.

References

Arveson, J. C., Weaver, E. C., and Millard, J. P. (1971) Rapid assessment of water pollution by airborne measurement of chlorophyll content, *AIAA Joint Conference of Remote Sensing of Environmental Pollutants*, Palo Alto, California, November.

Austin, R. W., (1974). Remote sensing of spectral radiance in *Optical Aspects of Oceanography* (N. G. Jerlov and E. Steeman, Eds.), Neilsen, Academic Press, London and New York, p. 371.

Clarke, G. L., Ewing, G. C., and Lorenzen, C. J. (1970), Spectra of backscattered light from the sea obtained from aircraft as a measure of chlorophyll concentrations, *Science*, **167**, 1119.

Gordon, H. R., (1973), Simple calculation of the diffuse reflectance of the ocean, *Appl. Opt.* **12**, 2830.

Gordon, H. R., and Brown, O. B., (1973) Irradiance reflectivity of a flat ocean as a function of its optical properties, *Appl. Opt.* **12**, 1549.

Gordon, K. S., (1975). The spectral and angular variation of sunlight backscattered from natural water, Ph.D. Thesis, York University, Toronto.

Grum, F., and Luckey, G. W. (1968), Optical sphere paint and a working standard of reflectance, *Appl. Opt.* **7**, 2289.

Jain, S. C., and Miller, J. R. (1976), Subsurface water parameters: optimization approach to their determination from remotely sensed water color data, *Appl. Opt.* **15**, 886.

Jain, S. C. Miller, J. R., and McNeil, W. R. (1975), An evaluation of a mathematical model for water colour spectral analysis, *Proc. 3rd Canadian Symposium of Remote Sensing*, Edmonton, Alberta, September 22-24, p. 289.

Jerlov, N. G., (1968), *Optical Oceanography*, Elsevier Publishing Co., Amsterdam, London and New York.

Kattawar, G. W., and Humphreys, T. J. (1976) Remote sensing of chlorophyll in an atmosphere - ocean environment: A theoretical study, *Appl. Opt.* **15**, 273.

McCluney, W. R. (1974), Ocean color spectrum calculations, *Appl. Opt.* **13**, 2422.

McNeil, W. R., and Thomson, K. P. B. (1974), Remote measurement of water colour and its application to water quality surveillance, *Proc. 3rd Symposium on Remote Sensing of Earth Resources*, (F. Shahrokhi, Ed.) Vol. **III**, VTSI, Tullahoma, Tenn.

McNeil, W. R., Thomson, K. P. B., and Jerome J. (1972) The application of remote spectral measurements to water quality monitoring, *Canadian J. Rem. Sens.* **2**, 49.

Miller, J. R., Gordon, K. S., and Kamykowki, D. (1976) Airborne water colour measurements of the Nova Scotia coast, *Canadian J. Rem. Sens.* **2**, 42.

Miller, J. R., Shepherd, G. G., and Koehler, R. A. (1971), A four channel scanning photometer for remote sensing, *Canadian Aeronaut. Space J.* **18**, 325.

Miller J. R., Shepherd, G. G., and Koehler, R. A. (1973) Airborne spectroscopic measurements over water, *Canadian Aeronaut. Space J.* **19**, 521.

Ramsey, R. C. and White, P. G. (July 1973) Ocean color analysis applied to MDCS and SIS data, NOAA contract report.

Received 22 November 1976; revised 10 March 1976